Medical Dosimetry, Vol. 27, No. 3, pp. 215–220, 2002

0958-3947/02/$–see front matter

PII: S0958-3947(02)00139-5

COMPENSATORS FOR INTENSITY-MODULATED BEAMS

D. M. DIMITRIADIS, M.SC., and B. G. FALLONE, PH.D., F.C.C.P.M., A.B.M.P.
Medical Physics Unit, McGill University Health Science Centre, Montreal, Canada; and Medical Physics, Cross Cancer Institute, University of Alberta, Edmonton, Canada

(*Accepted* 30 *August* 2001)

Abstract—This study describes the importance of attenuator scatter in the construction of compensators. The attenuator used in this study was Lipowitz metal, commonly referred to as cerrobend. Linear attenuation coefficients of cerrobend were measured in air for different thickness of cerrobend sheets and different field sizes for a 6-MV photon beam. The magnitude of the dose contribution from photons scattered by the attenuator was measured. The variations of beam hardening and the scatter to primary ratio as a function of the thickness of cerrobend and varying field size were investigated. The compensators in this study were produced using a simple exponential attenuation model and the measured linear attenuation coefficients. It was found that the beam hardening effect was significant, and can lead to an error of 6.2% in the transmission, for 6 cm of cerrobend in the beam. The maximum scatter contribution to the measured fluence was 19.8% of the transmitted primary dose for a 20 × 20-cm^2 field size, and 6 cm of cerrobend in the beam. For a simple wedge-step compensator; there was a maximum deviation of 6% between the measured and our predicted fluence profile. For simple compensators, this deviation can be attributed to scatter. **© 2002 American Association of Medical Dosimetrists.**

Key Words: **Compensators, Intensity-modulated beams, Attenuation model, Scatter, Penumbra.**

INTRODUCTION

Beam modifying filters such as wedges and compensators are used in radiotherapy to modify the dose distributions in externally applied photon beams. Further conforming the dose to the target volume necessitates the 3D modulation of the beam intensity, leading to the introduction of intensity-modulated radiation therapy (IMRT). There are many techniques by which one can deliver IMRT dose distributions. This work will focus on the use of photon beam compensators for the delivery of predetermined intensity distributions, and the importance of the scatter contribution due to the presence of the filter in the beam.

The introduction of compensators came at an early stage in radiotherapy, when it was realized that dose delivery could be improved through their use. Traditionally, compensation was introduced to preserve the shape of the isodose curves to account for an irregular patient surface, internal tissue heterogeneities, and sometimes beam obliquity.[1–3] Another use for compensators is for delivering IMRT beams. Compensators used for IMRT differ in their aim from traditional compensators. In IMRT, modulations with large changes in intensities must be achieved within the field, resulting in drastic thickness variation across the compensator. The thickness of a cerrobend compensator can be as great as 6 cm in some areas. For the purposes of intensity modulation, the effects of beam hardening and scatter with varying compensator thickness and field size were studied. A single effective attenuation coefficient cannot be used to construct the compensator with variable thickness of attenuator.[4] The presence of scattered photons may complicate the design compensators as well as the subsequent calculations of dose distributions.[5,6]

There are various methods by which compensators can be made. Commonly, compensators are made from molds filled with molten alloy or wax. The use of molds is advantageous because it results in compensators with smoother surfaces and thus greater accuracy. In this work, we quantify scatter in cerrobend compensators build in this way for intensity modulation.

THEORY

We used the technique reported by Huang *et al.*[7] to evaluate the scatter contribution due to the variation in cerrobend thickness. In this study, the attenuator is assumed to have a uniform thickness, t. The absorbed dose produced by the beam beyond the filter consists of a component, P, (which is smaller or equal to the dose due to the primary photons, P_0) and a component, S, due to scattered photons generated by the attenuator (Fig. 1). The secondary electrons produced by the attenuator are removed by the buildup cap of the detector and can thus be ignored.

The scattered component of the beam will not be detected in the case of "narrow beam" geometry created by small field sizes. Scatter-to-primary dose ratio (S/P) of the attenuated beam for large field sizes can be expressed as:

Reprint requests to: B. G. Fallone, Medical Physics, Cross Cancer Insitute, University of Alberta, 11560 University Avenue, Edmonton, AB Canada T6G 1Z2. E-mail: gino.fallone@cancerboard.ab.ca

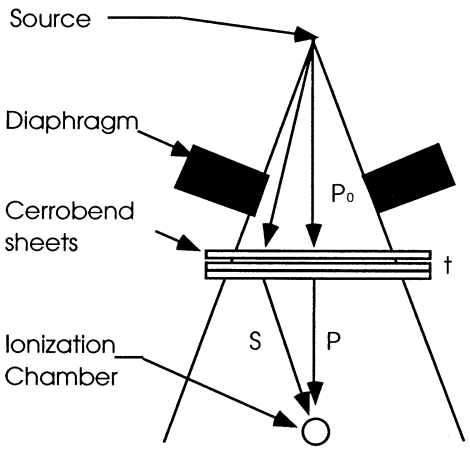

Fig. 1. Setup for measuring the dose contribution due to photons scattered by the filter.

$$\frac{S}{P} = \left[\frac{(S+P)}{P_0}\right]\left(\frac{P_0}{P}\right) - 1 \quad (1)$$

If I and I_0 are the detector signals measured with and without the filter, respectively, for a finite field size and i and i_0 are the measured values for a narrow-beam geometry, then we can substitute $\frac{(S+P)}{P_0}$ with $\frac{I}{I_0}$ and $\frac{P_0}{P}$ with $\frac{i_0}{i}$ in Eq. (2) to obtain

$$\frac{S}{P} \approx \left(\frac{I}{I_0}\right)\left(\frac{i_0}{i}\right) - 1 \quad (2)$$

We can define an effective attenuation coefficient for narrow-beam, μ_0, and broad-beam geometry, μ_b, respectively, in the following manner:

$$\mu_0 = -\frac{\ln\left(\frac{i}{i_0}\right)}{t} \quad (3)$$

where i is the electrometer reading with attenuator in the beam, and i_0 is electrometer reading without any attenuator for narrow-beam geometry.

$$\mu_b = -\frac{\ln\left(\frac{I}{I_0}\right)}{t} \quad (4)$$

Similarly, I is the electrometer reading with attenuator in the beam, and I_0 is the reading without any attenuator for broad-beam geometry. The term effective is used to reflect the polychromatic spectra of the beam.

From Eq. (2), the S/P can be defined in terms of μ_0 and μ_b.

$$\frac{S}{P} \approx e^{[(\mu_0-\mu_b)t]} - 1 \quad (5)$$

For thin attenuators, that is small values of t, Eq (5) can be further simplified and the S/P can be expressed as approximately equal to the difference between the narrow-and broad-beam attenuation coefficient multiplied by the thickness of the attenuator.

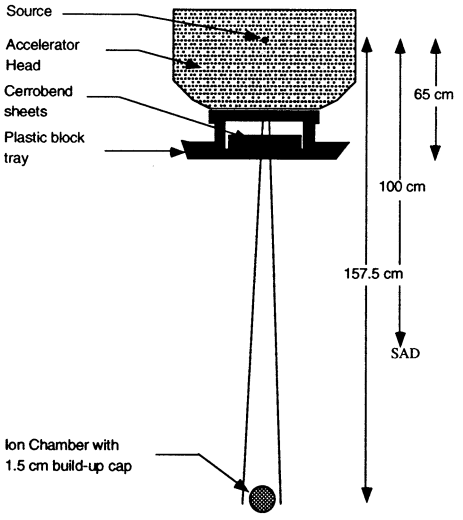

Fig. 2. Experimental setup for transmission measurements.

$$\frac{S}{P} \approx (\mu_0 - \mu_b) \cdot t \quad (6)$$

Therefore, we would expect the S/P to be proportional to the attenuator thickness for a considerable range.

MATERIALS AND METHODS

Measuring the narrow-beam attenuation coefficient

The narrow-beam attenuation coefficients were measured for the 6-MV photon spectrum from a Varian Clinac 2300 C/D (Varian Associates, Palo Alto, CA) linear accelerator. Narrow-beam attenuation coefficient measurements are ideally carried out at an extended source-to-surface distance (SSD) and for a small field size. Thus, a 3 × 3-cm^2 field size was used and the measurements were performed on the central axis for an SSD of 157.5 cm. Molds for this work were constructed with a computer numerically controlled (CNC) milling machine (Techno, ISEL, New Hyde Park, NJ). CNC mills can produce the complex surfaces required for IMRT compensation with good precision and accuracy.

The cerrobend (Cerro Metal Products, Belleforte, PA) thickness used varied from 0.3 to 6 cm, in 1-cm increments. Additional 0.3-cm steps were also used in the range of 1 to 2 cm. For the transmission measurements, the sheets were placed on the plastic block tray of the linac, located 65 cm from the photon source. An electrometer (Electrometer/Dosimeter #581) was used with a Shomca 781 ion chamber to take the measurements. These were done in air with a 1.5-cm radius polystyrene buildup cap on the chamber. The reading was recorded for different thicknesses of cerrobend, ranging from 0 to 6 cm. The set up is illustrated in Fig. 2. Measurements in this work were mainly done on the central axis.

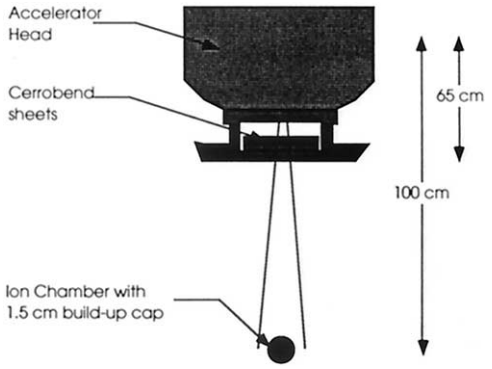

Fig. 3. Experimental setup for scatter measurements. Chen *et al.*[15] found scatter from the phantom to be significant. To avoid phantom scatter, all measurements were performed in air.

Evaluation of scatter contribution

A setup similar to the one used to measure the narrow-beam attenuation coefficients was used to assess the scatter contribution due to the presence of the attenuator in the beam. Instead of acquiring the measurements at extended SSD, they were taken at an SSD of 100 cm; the attenuator to chamber distance was 35 cm (Fig. 3). The increased presence of scattered photons due to this broad-beam geometry complicated the design of filters because scatter is influenced by the filter thickness, field size, distance from the filter, and distance from the central axis. The scatter variation for the first 3 cases was investigated in this work.

Evaluation of simple compensators

The evaluation of missing tissue compensators has been extensively reported in the literature.[8–11] Recently, the use and dosimetric evaluation of compensators for IMRT has also been studied.[12,14] We studied the errors associated with the use of the simple attenuation model for IMRT compensator construction, and observed if the scatter measurements, discussed earlier, accounted for the differences measured. The measurements were carried out for the 6-MV beam at source-to-axis distance

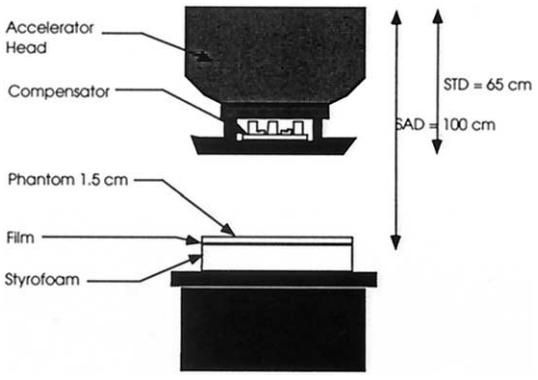

Fig. 4. Experimental setup for the evaluation of compensators.

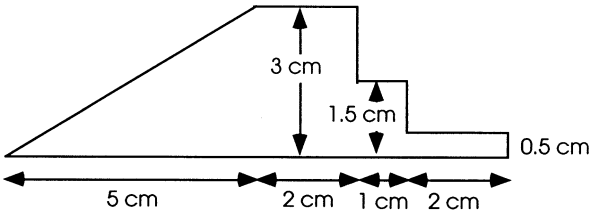

Fig. 5. Simple wedge-step compensator.

(SAD) of 100 cm, with only enough phantom material to assure dose buildup at the measuring plane.

The measurements were carried out for a source-to-tray distance of 65 cm and a field size of 15.4×15.4 cm^2 (Fig. 4). A simple wedge-step compensator was used to test the prediction of the simple attenuation model (Fig. 5).

RESULTS AND DISCUSSION

Narrow-beam attenuation coefficient

Generally, a filter hardens the beam by preferentially attenuating the lower-energy photons of a polyenergetic beam. The effect of beam hardening[8] can be assessed by observing the variation in the measured attenuation coefficients with thickness of cerrobend. The variation of the narrow-beam attenuation coefficient with increasing cerrobend thickness is shown in Fig. 6. The narrow-beam attenuation coefficient, μ_t, was calculated for each thickness using the following formula:

$$\mu_t = -\frac{\ln \frac{I_t}{I_0}}{t} \tag{7}$$

where I_t and I_0 is the reading with and without an attenuator of thickness t cm in the beam, respectively.

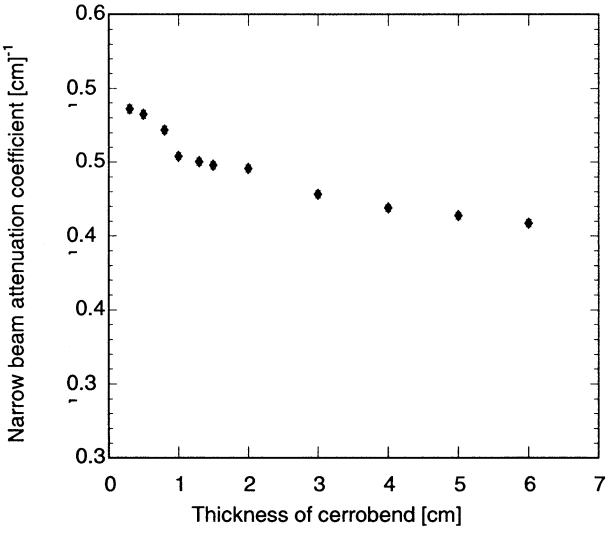

Fig. 6. Measured narrow-beam linear attenuation coefficient vs. thickness of cerrobend.

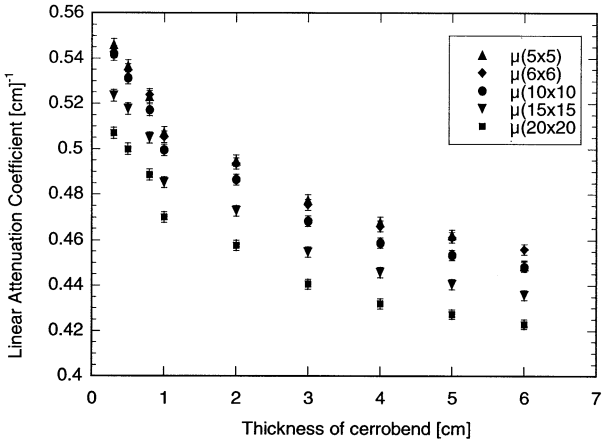

Fig. 7. Measured linear attenuation coefficient vs. thickness of cerrobend for different field sizes.

The measured attenuation coefficient decreases with increasing thickness of attenuator because the average energy of the beam increases with thickness of attenuator.

The "hardening" effect of the beam by the attenuator must be considered because compensators for IMRT involve great variations in thickness. According to Fig. 6, the measured narrow-beam attenuation coefficient changes by 0.01 cm^{-1} per cm of cerrobend, which causes a maximum change of 6.2% in attenuation for a thickness of 6 cm. Because the scatter from the attenuator is negligible at extended SSD, the variation in the measured attenuation coefficient is mainly due to beam hardening.

Evaluation of scatter contribution

Measurements of the attenuation coefficients were carried out for the various field sizes in Figs. 7 and 8. The measured effective attenuation coefficients for the field sizes 5 × 5 cm^2 and 6 × 6 cm^2 are indistinguishable.

The data points for a 5 × 5-cm^2 field represent the

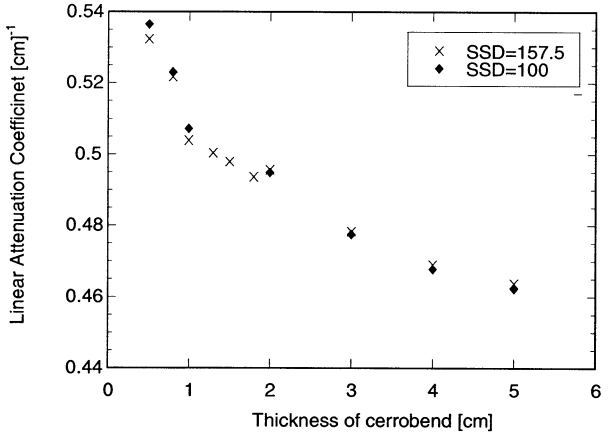

Fig. 8. Linear attenuation coefficient vs. thickness of cerrobend for narrow-beam geometry, field size 3 × 3 cm^2 for SSD = 157.5 cm and field size 5 × 5 cm^2 for SSD = 100 cm.

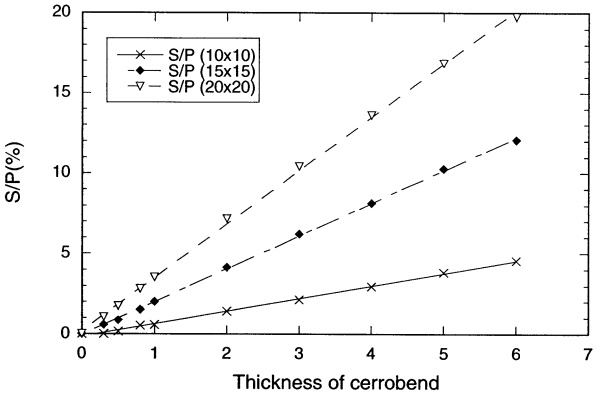

Fig. 9. Percentage scatter vs. thickness of filter for different field sizes.

narrow-beam effective attenuation coefficient, μ_0, in Eq. (3). The narrow-beam effective attenuation coefficient decreases as the thickness of attenuating filter increases, attesting to the progressive hardening of the x-ray beam, as discussed above. The broad-beam attenuation coefficient varies in a similar manner for larger field sizes with filter thickness. It is also interesting to note that the value of the broad-beam attenuation coefficient decreases as the field size increases. The difference between the effective attenuation coefficient for a 5 × 5-cm^2 field and that of a 20 × 20-cm^2 field is 8%. This difference is constant for all cerrobend thickness.

We use the narrow-beam geometry as standard for our analysis because of the reduced amount of scatter involved. The narrow-beam coefficients (field of 5 × 5 cm^2) that we measured at an SSD of 100 cm were compared with the previous measurements at an extended SSD of 157.5 cm. The maximum difference measured was 2.2% of μ_0 at extended SSD (Fig. 5). Therefore, we can conclude that the scatter contribution produced in the filter with narrow field size is small and does not influence the measurement of i/i_0 at any distance. The error in all measurements was too small to be shown on the plots.

The S/P was calculated for the above field sizes using the broad-beam attenuation coefficient and Eq. (6). A plot of the percentage scatter vs. the thickness of filter is illustrated in Fig. 9. Because the slope of the plot ($\mu_0 - \mu_b$) is essentially constant, *S/P* is directly proportional to compensator thickness.

Scattered photons may contribute to significant dose errors of up to 20%. The exact contribution depends on the amount of material in the beam and the field size. For a case of a 10 × 10-cm^2 field size, for example, the scatter is 4.6% for a thickness of 6 cm of attenuator, as can be deduced from Fig. 9. The S/P was found to increase with field size and thickness of compensator. For a 20 × 20-cm^2 field size, the percentage S/P is as high as 19.8%. The scatter contribution is of significance for IMRT compensators because the compensator can

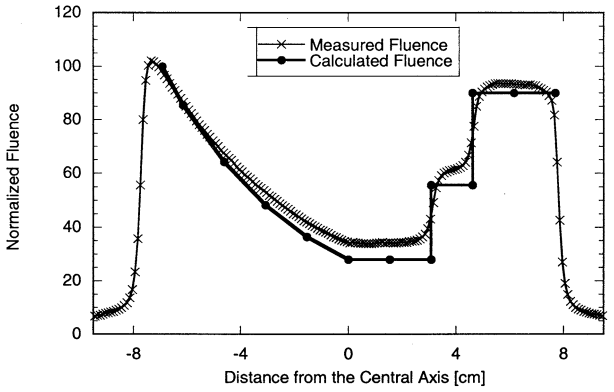

Fig. 10. Measured and predicted fluence distribution for the wedge-step compensator.

contain thicknesses of up to 6 cm. Scatter is expected to be less significant with distance from the central axis.[7] The resulting maximum change in transmission (I/I_0) is 6.4% for 6 cm of cerrobend. The effect of beam hardening can be accounted for by using the appropriate attenuation coefficient for each thickness value.

Evaluation of simple compensators

Compensators were evaluated by comparing the predicted fluence distribution using the simple attenuation model, Eq. (7), with the fluence distribution measured with film for the narrow-beam linear attenuation coefficients at extended SSD for the different thickness of cerrobend (Fig. 10).

The fluence was measured for the wedge-step compensator and compared to that predicted (Fig. 11). The measured and predicted fluence distributions agree very well when the normalized fluence is above 70%, that is, they agree very well for small thickness' of cerrobend ($<$ 1.5 cm) where the percentage of S/P is of the order of 3% or less for a 15×15-cm^2 field. At a distance of 1.07 cm from the central axis, the deviation between the predicted and measured fluence is 6.04%. The measured percentage S/P for a field size of 15×15 cm^2 for a thickness of 3 cm of cerrobend is 6.20% (Fig. 9). This illustrates that the deviation observed between the magnitude of the predicted fluence and that measured can be primarily attributed to scattered radiation.

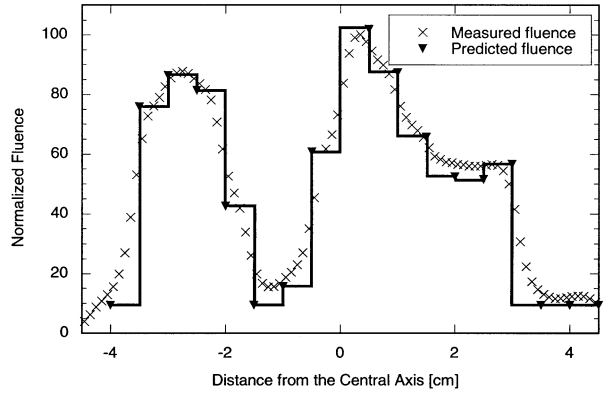

Fig. 11. Normalized fluence vs. distance from central axis for arbitrary fluence profile.

Stepped compensator

Using the same setup as for the wedge-step compensator, a stepped compensator was also tested. The field size was set at 8.5×8 cm^2. The normalized predicted fluence is compared with the normalized measured fluence (Fig. 11). It must be noted that it is very difficult to achieve a fluence distribution with the sharp variations.

The maximum deviation between the measured and predicted fluence from which the compensator is designed is 6.53% at a distance of -1.27 cm from the central axis. This can be partly attributed to the scatter, which was measured to be 4.5% of the primary.

In a case of a stepped distribution, the study of the penumbra associated with each sharp modulation between steps is difficult. These difficulties will remain, especially at off-axis positions, for large thickness' compensators.

CONCLUSIONS

The presence of scattered photons leads to only minor errors in the clinical applications of simple missing tissue compensators. However, scattered photons from compensators used for intensity modulation introduce significant errors. It was found that the compensator hardens as well as scatters the beam in a nonuniform way, depending on the thickness and the shape of the compensator. The compensator thickness profile can be simply calculated from the optimized primary fluence profile without taking into account the beam perturbations caused by the compensator. The error introduced when using the simple attenuation model to determine the thickness profile of the compensator can be of the order of 20% for a 20×20-cm field and 6 cm of cerrobend in the beam. Scatter was found to be negligible in the case of very small fields (5×5 cm).

REFERENCES

1. Clark, B.G.; Evans, M.D.C. Standard compensators for ENT therapy fields. *Med. Dosim.* **13:**173–7; 1988.
2. Shragge, P.C.; Patterson, M.S. Improved methods for the design of tissue compensators. *Med. Phys.* **8:**885–91; 1981.
3. Renner, W.D.; O'Connor, T.P.; Bermudez, N.M. A note on designing tissue compensators for parallel opposed fields. *Med. Phys.* **10:**483–6; 1983.
4. Boyer, A.L. Compensating filters for high energy x rays. *Med. Phys.* **9:**429–33; 1982.
5. Robinson, D.M.; Scrimger, J.W. Limitation of retracted missing tissue compensators: An experimental analysis. *Med. Dosim.* **14:** 49–54; 1989.
6. Ansbacher, W.; Robinson, D.M.; Scrimger, J.W. Missing tissue compensators: Evaluation and optimization of a commercial system. *Med. Phys.* **19:**1267–72; 1992.
7. Huang, P.; Chin, L.M.; Bjärngard, B.E. Scattered photons produced by beam-modifying filters. *Med. Phys.* **13:**57–63; 1986.

8. Chu, T.; Lee, K.; Dunscombe, P. A technique for the evaluation of a missing tissue compensator system. *Med. Phys.* **20:**713–6; 1993.
9. Low, D.A.; Li, Z.; Klein, E.E. Verification of milled two-dimensional photon compensating filters using an electronic portal imaging device. *Med. Phys.* **23:**929–38; 1996.
10. Basran, P.S.; Ansbacher, W.; Field, G.C.; Murray, B.R. Evaluation of optimized compensators on a 3D planning system. *Med. Phys.* **25:**1837–44; 1998.
11. Ansbacher, W.; Robinson, D.M.; Scrimger, J.W. Missing tissue compensators: Evaluation and optimization of a commercial system. *Med. Phys.* **19:**1267–72; 1992.
12. Levegrün, S.; Hartwig, K.; Oelfke, U.; et al. Clinical implementation of intensity-modulated treatments using compensators: Dosimetric verification. *Med. Phys.* **25:**A150; 1998.
13. Jiang, S.B.; Ayyangar, K.M. On compensator design for photon beam intensity-modulated conformal therapy. *Med. Phys.* **25:**668–75; 1998.
14. Sewchand, W.; Khan, F.M.; Williamson, J. Variation in depth dose data between open and wedge fields for 4 MV x-rays. *Radiology* **3:**789–92; 1978.
15. Chen, Z.; Wang, X.; Bortfeld, T.; Mohan, R.; Reinstein, L. The influence of scatter on the design of optimized intensity modulations. *Med Phys*. **22:**1727–1733; 1995.